Improved photocatalytic properties of ZnS/RGO nanocomposites prepared with GO solution in degrading methyl orange

Yanli Qin [a,b], Zheng Sun [a,b], Wenwen Zhao [a,b], Zhenyu Liu [b], Dingrui Ni [b,*], Zongyi Ma [b,**]

[a] School of Science, Shenyang Ligong University, No.6 Nanping Central Road, Shenyang 110159, China
[b] Shenyang National Laboratory for Materials Science, Institute of Metal Research, Chinese Academy of Sciences, 72 Wenhua Road, Shenyang 110016, China

HIGHLIGHTS

- ZnS/RGO nanocomposites were synthesized with GO aqueous solution as precursor.
- ZnS nanoparticles were uniformly loaded on the surface of graphene sheets.
- ZnS/RGO exhibited higher photocatalytic activity compared to pure ZnS.
- Surface reaction rate constant of ZnS/RGO was six times higher than pure ZnS.

GRAPHICAL ABSTRACT
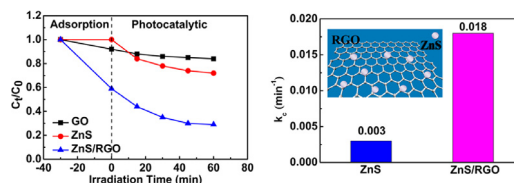
ARTICLE INFO

ABSTRACT

Zinc sulfide/Reduced graphene oxide (ZnS/RGO) nanocomposites were synthesized via one-step solvothermal method with commercial graphene oxide (GO) aqueous solution as precursor. The crystal structure and morphology of the ZnS/RGO nanocomposites were characterized by X-ray diffraction (XRD) and transmission electron microscopy (TEM), respectively. During the process GO was reduced into RGO and ZnS nanoparticles with a diameter of about 5 nm were uniformly loaded on the surface of graphene sheets. The smaller size and uniform distribution of ZnS nanoparticles benefited from the higher purity and smaller size of GO in aqueous solution. The photocatalytic activity of the nanocomposites was investigated through the photocatalytic degradation of methyl orange in aqueous solution. The ZnS/RGO nanocomposites exhibited higher photocatalytic activity compared to pure ZnS; furthermore, the surface reaction rate constant of the nanocomposites was six times higher than that of the pure ZnS.

© 2017 Elsevier B.V. All rights reserved.

1. Introduction

In the past couple of decades, semiconductor nanostructures have been a subject of extensive interest due to their fundamental importance as well as enormous potential in optoelectronic, magnetic, and catalytic applications [1–3]. The optical catalysts of semiconductor have received much attention in the field of organic pollutant degradation research because these catalysts can convert light energy into chemical energy without regenerating pollution in the environment [4,5]. Photocatalyst is generally based on the light absorption of semiconductor to excite the electrons from valence band to conduction band, creating electron–hole pairs. These electrons and holes can transfer to the surface of materials and generate a series of redox reactions with water and oxygen molecules, degrading organic molecules adsorbed on the surface of the photocatalyst [6].

As one of typical II–VI semiconductor materials with a wide direct band gap (3.6 eV), zinc sulfide (ZnS) has received considerable concern due to its excellent properties such as strong oxidation

and lower secondary pollution. So far, various ZnS heterogeneous nanostructures have been used to degrade the harmful dyes into less harmful chemicals by photocatalytic reaction under ultraviolet (UV) light illumination.

Given its photocatalytic properties, ZnS is a popular research topic [7]; however, its photocatalytic efficiency is not high enough as a result of the fast recombination of photo-generated electron–hole pair. This feature severely limits its practical application in the environmental protection. Extensive investigations showed that combining the traditional photocatalysts with other carrier materials could effectively reduce the recombination of photogenerated electron–hole pairs, such as precious metals [8,9], compound semiconductors [10,11], and carbon materials [12].

Carbon materials are increasingly becoming a popular choice for the formation of composites with semiconductor nano materials. The purpose of this compound is to combine excellent photocatalytic properties of conventional semiconductor photocatalysts with excellent electrical and optical properties of carbon materials. Graphene with unique physical and chemical properties associated with their two-dimensional (2D) single monolayer form of sp^2 carbon atoms arranged in a honeycomb lattice, has attracted tremendous attention from theoretical and experimental scientists [13–17].

Graphene, including graphene oxide (GO) and reduced graphene oxide (RGO), is introduced and integrated with semiconductor photocatalysts due to its unique properties, such as high electronic conductivity (16 000 S/m), high specific surface area (2600 m^2/g, theoretical value), and regular 2D planar structure. On the one hand, graphene could limit the agglomeration of nanoparticles, thereby increasing the number of effective active reaction sites. On the other hand, it can accelerate the charge transferring from the photocatalyst to the liquid–solid interface contacting with organic pollutants by taking advantage of the unique electron transport property of graphene [18,19]. In this process, the photocatalytic performance of the composite catalyst can be improved. So far, more and more efforts have been paid on the research and development of the photocatalyst/Graphene nanocomposites such as TiO_2/RGO [20–22], BiOCl/RGO [23], ZnO/RGO [24–26], ZnS/RGO [27,28], etc.

"One-step solvothermal method" is one of the main techniques for preparing carbon-semiconductor nanocomposites. In this method, conventional solid graphite powder was usually adopted as a precursor. As a potential alternative with excellent properties, graphene especially GO might be more suitable for preparation of carbon-semiconductor nanocomposites compared to the graphite powder because the surface of GO has a variety of functional groups which can absorb more nanoparticles. In particular, the GO aqueous solution can be applied to mass production. Therefore, it is of great significance for the preparation of photocatalytic nanocomposites with higher quality by using GO aqueous solution [29–32].

In this study, ZnS/RGO nanocomposites were synthesized via a single-step solvothermal method with GO aqueous solution as the precursor. Furthermore, the photocatalytic performance of the nanocomposites was evaluated by degrading methyl orange (MO) solution under UV light illumination.

2. Experimental

2.1. Materials

GO aqueous solution (2 mg/ml) was purchased from the Shanxi Coal Research Institute, Chinese Academy of Sciences. Zinc acetate, sodium sulfide, methyl orange, ethylene glycol, and anhydrous ethanol were purchased from Sinopharm Chemical Reagent Co., Ltd, and used without further purification. All laboratory reagents

employed in the analysis were pure with deionized water utilized in all experiments.

2.2. Preparation of ZnS/RGO nanocomposites

Fig. 1 shows the schematic diagram for the preparation of the ZnS/RGO nanocomposites. In a typical synthesis process, ZnS/RGO nanocomposites were prepared with the solvothermal method by using ethylene glycol as a solvent. 100 mg of zinc acetate dihydrate was first dissolved into 20 ml of ethylene glycol. Then, 20 ml (2 mg/ml) GO aqueous solution was added into the solution and subjected to ultrasonic treatment for 30 min to produce a light brown solution. Subsequently, 100 mg of sodium sulfide was added into 20 ml solvents under ultrasonic treatment. This solution was then added into the previously light brown solution and the mixture was stirred for 30 min. Finally, the mixture was autoclaved in a Teflon-lined stainless steel vessel at 180 °C for 10 h. The reaction products were centrifuged and washed with deionized water and anhydrous ethanol, and then dried in a vacuum oven at 60 °C.

2.3. Photocatalytic performance experiments

The photocatalytic activity levels of the ZnS/RGO nanocomposites were estimated by monitoring the degradation of MO in a self-assembled apparatus with a UV lamp (8 W) as the radiation source. Typically, 20 mg of photocatalysts is suspended in a beaker containing an aqueous solution that consists of model dye (50 mL; 20 mg/L) in the photocatalytic experiment. First, the suspension was subjected to ultrasonic treatment for 30 min to reach adsorption–desorption equilibrium without UV light exposure (adsorption region: −30–0 min). Subsequently, a photocatalytic reaction was initiated by UV light irradiation with continuous magnetic stirring (photocatalytic region: 0–60 min). At specific time intervals, 3 ml suspensions were sampled and centrifuged. Then, the supernatants were collected for analysis with the UV–vis absorption spectrometer.

The intensity of the maximum absorption peak (463 nm) of the MO dye was regarded as a measure of residual MO dye concentration. According to Lambert–Beer law, $C_t/C_0 = A_t/A_0$, where C_0 is the concentration of the MO solution after dark adsorption; C_t is the concentration of the MO solution after illumination time t; A_0 is the absorbance of the MO solution after dark adsorption; A_t is the absorbance of the MO solution after illumination time t.

2.4. Microstructural and spectrum characterization

The phase and crystallite size of the ZnS/RGO composites were characterized with an automated X-ray powder diffractometer (XRD, Rigaku D/max 2400) with a monochromated CuKα radiation (λ = 0.154056 nm). The surface morphology, particle size, and composition of samples were examined using transmission electron microscopy (TEM, TECNAI 20). The UV–vis absorption spectrum was recorded with a UV–vis spectrophotometer (INESA, UV757CRT/PC).

3. Results and discussion

3.1. Characteristics of ZnS/RGO nanocomposites

The XRD patterns of the ZnS/RGO nanocomposites are shown in Fig. 2. As can be seen, three relatively strong peaks appeared around 28.61°, 47.62° and 56.51°, which are assigned to (111), (220) and (311) reflections of the sphalerite ZnS (JCPDS 05-0566). The crystallinity of ZnS in the nanocomposites (Fig. 2(c)) is close to that of the pure ZnS sample without characteristic peaks assigned
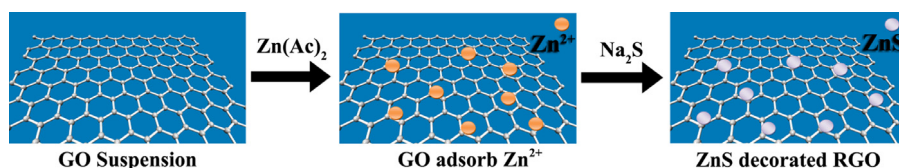
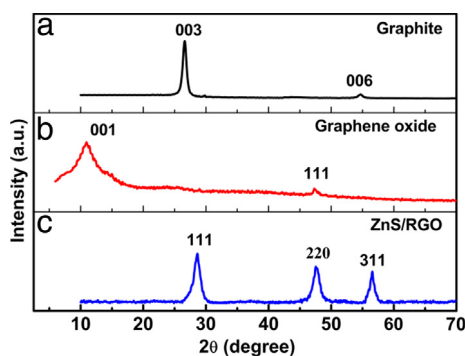**Fig. 1.** Proposed scheme for fabrication processes of ZnS/RGO.

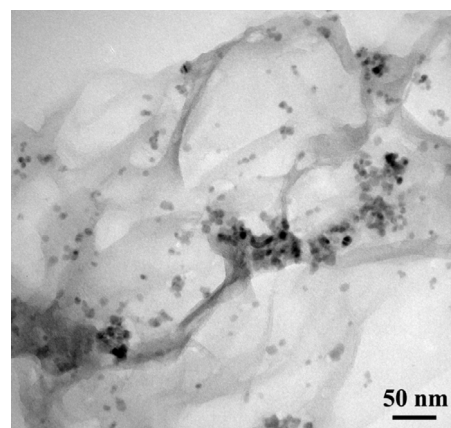**Fig. 2.** XRD patterns of ZnS/RGO nanocomposites.

Fig. 3. TEM images of ZnS/RGO nanocomposites.

to the graphite sample (Fig. 2(a)) or graphene oxide (Fig. 2(b)). This indicates that the existence of RGO did not affect the growth of ZnS, thus RGO only functioned as a platform where the ZnS nanoparticles could nucleate and grow as well.

It has been reported that, if the regular stacks of GO or graphene were destroyed, for example by exfoliation, their diffraction peaks would become weak or even disappear [33]. It is worth noting that the crystallinity of the sample is a key factor in the use of its photocatalytic properties, and higher crystallinity may produce better photocatalytic activity. In addition, according to the half height width β and the diffraction angle θ of the (111) crystal plane, the average grain size of ZnS in the composites was estimated to be about 5 nm using the Scherrer formula ($d = 0.89\lambda/\beta\cos\theta$).

The morphological characteristics of ZnS/RGO nanocomposites are shown in Fig. 3. It can be seen that ZnS nanoparticles were uniformly distributed on the surface or edge of the graphene sheets, and two dimensional structures with surface wrinkles of the graphene sheet could be clearly distinguished. The diameter of the ZnS nanoparticles was about 5 nm, which is consistent with the average grain size calculated by Scherrer formula. It is noted that some tiny ZnS nanoparticles gathered together and distributed randomly on the surface of the graphene sheets. It is considered that graphene sheets played an important role in promoting the nucleation and growth of the ZnS nanoparticles, and the agglomeration of the ZnS particles could be effectively prevented by using graphene sheets [34].

Based on the above results, the formation mechanism of ZnS/RGO nanocomposites can be described as follows. Firstly, the Zn^{2+} ions gather on the negatively charged GO surface. Secondly, the hydrothermal process results in the reaction of adsorbed Zn^{2+} on GO with S^{2-} ions to generate the initial ZnS nuclei. Thirdly, an *in situ* charge transfer process occurs from the ZnS nuclei to the GO when the reductions of GO take place. Due to the large specific surface area and high concentration of RGO sheets in solution, a large number of tiny primary nanoparticles tend to condense and aggregate to form larger particles. So, after the fast nucleation period, the mechanism of aggregation is mostly related to random agglomeration [35].

The synthesis of ZnS/graphene nanocomposites with graphite powders as raw material has been reported previously [36,37]. However, in these investigations ZnS nanoparticles showed a diameter size of about 11–42 nm, and the agglomeration of nanoparticles were observed; meanwhile, the ZnS particles appeared mainly on the edges and wrinkles, but rarely on the smooth parts of the graphene sheets, which would be correlated with the more abundant oxygen-containing functional groups on the these sites than the smooth parts [37]. Furthermore, it should be mentioned that another possible reason of this phenomenon is the large size of the graphene sheets which were made directly from graphite powder [37].

Compared to results of Refs. [36,37], in the present study, the ZnS nanoparticles showed a smaller size (∼5 nm) and were uniformly distributed on the surface of the graphene sheets by using GO aqueous solution due to its higher purity and smaller size. Recently, Azimi et al. [27] investigated the effect of graphene concentration on the photovoltaic and UV detector applications of ZnS/RGO composites, which were synthesized with different graphene concentrations (5, 10, and 15 wt%) using high purity GO powders as a graphene source. Their result showed that by increasing the RGO concentration, the average size of ZnS nanoparticles decreased, ∼45 nm and ∼9 nm for the 5 wt% and 15 wt% concentration, respectively, and the latter is similar to the result of the present study. These results indicates that compared to the raw material of graphite powders, the higher purity and smaller size of GO in aqueous solution could benefit the smaller size and uniform distribution of ZnS nanoparticles.

3.2. Photocatalytic properties of ZnS/RGO nanocomposites

Fig. 4(a) shows the photocatalytic properties of the ZnS/RGO nanocomposites compared to other samples under UV irradiation conditions. The pure GO sample substantially exhibited no photocatalytic activity, but it showed partial degradation effect because of its great specific surface area which absorbed part of organic dye molecules. The normal ZnS sample had certain photocatalytic degradation ability; however, for this sample, the UV light induced photo-generated electron–hole pairs are easy to recombine, which seriously limits its quantum efficiency and reduces the efficiency of photocatalytic degradation. It is seen that the photocatalytic degradation efficiency of the nanocomposites was significantly improved compared with the pure ZnS and pure graphite samples. Fig. 4(b) is the UV–vis absorption spectrum of
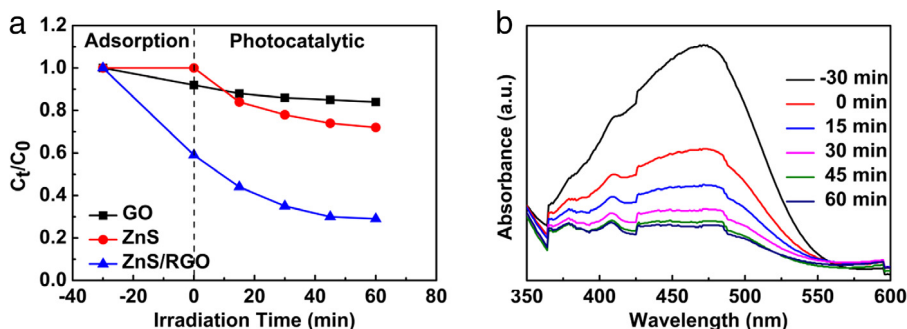
Fig. 4. (a) Photocatalytic degradation curves of methyl orange in the presence of ZnS and ZnS/RGO nanocomposites under UV light irradiation, (b) UV–vis absorption spectra of MO degraded by ZnS/RGO nanocomposites within different times.

the MO dyes degraded by the nanocomposites within 60 min, the intensity of the maximum absorption peak (463 nm) of the MO dye was referred to as a measure of the residual MO dye concentration according to the Lambert-beer's law.

It should be pointed out that the organic dye molecules adsorbed on the surface of the nanocomposites and photocatalytic degradation of organic dye molecules are the two inseparable and mutually promoted processes (Fig. 4(a), adsorption region: −30–0 min, photocatalytic region: 0–60 min). On the one hand, a lot of contaminant molecules are adsorbed on the surface of graphene due to its unique two-dimensional structure and great specific surface area, which soon reach the adsorption equilibrium in the photocatalytic reaction system. Then, the adsorption equilibrium of pollutant molecules adsorbed on the surface of graphene is destroyed by the oxidation reaction which degrades the organic pollutants. Immediately, the organic pollutant molecules in the solution will be continuously adsorbed on the surface of the composites, reaching a new dynamic equilibrium, and eventually being photocatalytic degraded due to ultraviolet radiation effect.

On the other hand, the photo-generated carriers can be effectively separated by graphene modified treatment, because of the photo-generated electrons can be effectively transferred to other positions on the surface of graphene sheets by taking advantage of its unique electron transport property; therefore, the quantum yield is significantly improved. Photo-generated electrons and holes further react to generate a variety of active substances, followed by oxidative degradation of organic dye molecules which adsorbed on the surface of the nanocomposites. As a result, based on the synergistic effect of adsorption–photocatalytic degradation, the nanocomposites showed a significantly enhanced photocatalytic activity.

Photocatalytic reactions on the ZnS/RGO nanocomposites surface can be expressed by the Langmuir–Hinshelwood model [38]. The photocatalytic degradation of MO by the nanocomposites under UV light obeyed pseudo-first order kinetics with respect to the concentration of MO:

$$\ln(C_0/C_t) = K_c \times t \qquad (1)$$

where K_c is the surface reaction rate constant, used as the basic kinetic parameter for different photocatalysts. The surface reaction rate constant values could be deduced from the linear fitting of $\ln(C_0/C_t)$ vs. t. The surface reaction rate constant for different catalysts are presented in Fig. 5. These results showed that K_c was enhanced by the introduction of graphene, and the surface reaction rate constant of the ZnS/RGO nanocomposites was six times higher than that of pure ZnS [6].

The photocatalytic degradation mechanism of organic dyes by the semiconductor catalyst under UV light irradiation is illustrated in Fig. 6. The mechanism is based on the excitation of the semiconductor. Valence electrons of ZnS can be excited to the conduction band owing to its sufficiently narrow band gap,
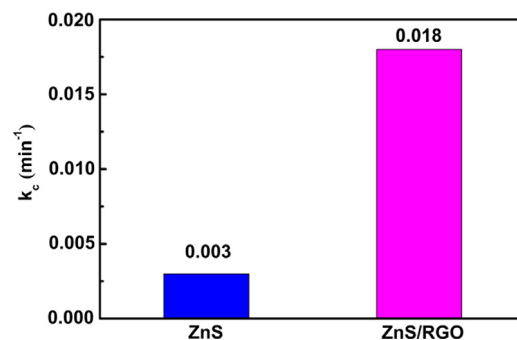
Fig. 5. Surface reaction rate constant of methyl orange photodegradation in the presence of ZnS/RGO nanocomposites under UV light irradiation.
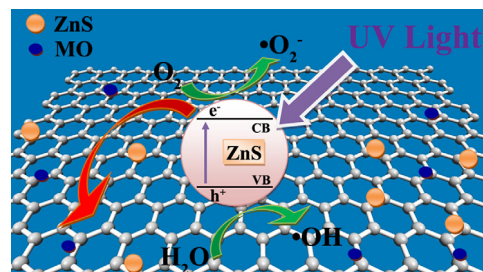
Fig. 6. Mechanism for the photodegradation of MO by ZnS/RGO nanocomposites under UV light irradiation.

leaving behind a hole in the valance band by absorbing UV light. When the photo-generated electron–hole pair is migrated on the surface of the ZnS nanoparticles through the internal electric field of the semiconductor, the photo-generated electrons react with dissolved oxygen molecules and produce active oxygen radicals, and the photo-generated hole can react with the hydroxide ion derived from water to form hydroxyl radicals. These oxygen peroxide radicals and hydroxyl radicals generated from the nanocomposites can cause the oxidative decomposition of MO to CO_2, H_2O, and other mineralization products, achieving the degradation effect.

According to the literatures [39–41], the enhancement of the photocatalytic degradation properties of the ZnS/RGO nanocomposites can be attributed to two aspects. Firstly, graphene has unexpectedly excellent conductivity due to its two dimensional planar structure; therefore, the rapid transport of photo-generated carriers could be achieved, and an effective charge separation is subsequently accomplished. Secondly, graphene is capable of adsorbing organic dye molecules on the surface of graphene sheets by its great specific surface area with a large number of π–π conjugated double bonds. Thus, the oxygen peroxide radicals and hydroxyl radicals generated from the ZnS/RGO nanocomposites degrade the MO dye in the ultraviolet irradiation.

Recently, for the application in the solar energy conversion, Zhang et al. [42] reported the assembly of nanosized ZnS particles on the GO sheet by a two-step wet chemistry process (during which the RGO, also called GR, were achieved). They reported that graphene could transform the wide band gap ZnS to a visible light photocatalyst due to the new role of graphene as a macromolecular photosensitizer. The ZnS/GR nanocomposites exhibited visible light photoactivity toward aerobic selective oxidation of alcohols and epoxidation of alkenes under ambient conditions. They proposed a new photocatalytic mechanism for the structure-photoactivity correlation analysis, in which the role of GR acted as an organic dye-like macromolecular "photosensitizer" for ZnS instead of an electron reservoir. Considering the microscopic charge carrier transfer pathway connected to the interface between the GR and the semiconductor, this concept could provide a new thought on designing GR-based composite photocatalysts for targeting applications not only in the solar energy conversion [42], but also in degrading organic pollutant as confirmed in the present study. And the photocatalytic degradation behavior of the ZnS/RGO nanocomposites on organic dyes under visible light irradiation will be investigated in the future.

4. Conclusions

ZnS/RGO nanocomposites photocatalysts were successfully synthesized by a single step solvothermal method in ethylene glycol medium. ZnS nanoparticles with a diameter of ~5 nm were deposited on the surface of graphene sheets. During the deposition process, graphene oxide was simultaneously reduced into RGO with the solvent thermal reaction, and the presence of graphene promoted the crystallization of ZnS nanoparticles. The enhancements of photocatalytic performance of the ZnS/RGO nanocomposites can be attributed to the efficient charge separation and enhanced adsorption capacity of the nanocomposites with the introduction of graphene. Compared with pure ZnS sample, the ZnS/RGO nanocomposites showed excellent photocatalytic properties. Photocatalytic reactions on the ZnS/RGO surface can be expressed by the Langmuir–Hinshelwood model, and their surface reaction rate constant was six times higher than that of pure ZnS sample.

Competing financial interests

The authors declare no competing financial interests.

References

[1] T. Mokari, E. Rothenberg, I. Popov, R. Costi, U. Banin, Selective growth of metal tips onto semiconductor quantum rods and tetrapods, Science 304 (2004) 1787–1790.
[2] W.T. Yao, S.H. Yu, X.Y. Huang, J. Jiang, L.Q. Zhao, L. Pan, J. Li, Nanocrystals of an inorganic-organic hybrid semiconductor: formation of uniform nanobelts of [ZnSe](diethylenetriamine)$_{0.5}$ in a ternary solution, Adv. Mater. 17 (2005) 2799–2802.
[3] D.H. Son, S.M. Hughes, Y.D. Yin, A.P. Alivisatos, Cation exchange reactions-in ionic nanocrystals, Science 306 (2004) 1009–1012.
[4] O. Kozak, P. Praus, K. Koci, M. Klementova, Preparation and characterization of ZnS nanoparticles deposited on montmorillonite, J. Colloid Interface Sci. 352 (2010) 244–251.
[5] D.H. Xiang, Y.B. Zhu, Z.J. He, Z.S. Liu, J. Luo, A simple one-step synthesis of ZnS nanoparticles via salt-alkali-composited-mediated method and investigation on their comparative photocatalytic activity, Mater. Res. Bull. 48 (2012) 188–193.
[6] M. Ahmad, E. Ahmed, Z.L. Hong, J.F. Xu, N.R. Khalid, A. Elhissi, W. Ahmed, A facile one-step approach to synthesizing ZnO/Graphene composites for enhanced degradation of methylene blue under visible light, Appl. Surf. Sci. 274 (2013) 273–281.
[7] G.Z. Shen, Y. Bando, J.Q. Hu, D. Golberg, Single-crystalline trumpetlike zinc phosphide nanostructures, Appl. Phys. Lett. 88 (2006) 143105.
[8] T. Hirakawa, P.V. Kamat, Charge separation and catalytic activity of Ag@TiO$_2$ core–shell composite clusters under UV-irradiation, J. Am. Chem. Soc. 127 (2005) 3928–3934.
[9] V. Subramanian, E.E. Wolf, P.V. Kamat, Catalysis with TiO$_2$/gold nanocomposites effect of metal particle size on the fermi level equilibration, J. Am. Chem. Soc. 126 (2004) 4943–4950.
[10] S.H. Elder, F.M. Cot, Y. Su, S.M. Heald, A.M. Tyryshkin, M.K. Bowman, Y. Gao, A.G. Joly, M.L. Balmer, A.C. Kolwaite, K.A. Magrini, D.M. Blake, The discovery and study of nanocrystalline TiO$_2$-(MoO$_3$) core–shell materials, J. Am. Chem. Soc. 122 (2000) 5138–5146.
[11] T. Tatsuma, S. Saitoh, P. Ngaotrakanwiwat, Y. Ohko, A. Fujishima, Energy storage of TiO$_2$-WO$_3$ photocatalysis systems in the gas phase, Langmuir 18 (2002) 7777–7779.
[12] A.M. Turek, I.E. Wachs, E. DeCanio, Acidic properties of alumina-supported metal oxide catalysts: an infrared spectroscopy study, J. Phys. Chem. 96 (1992) 5000–5007.
[13] K.S. Novoselov, A.K. Geim, S.V. Morozov, D. Jiang, Y. Zhang, S.V. Dubonos, I.V. Grigorieva, A.A. Firsov, Electric field effect in atomically thin carbon films, Science 306 (2004) 666–669.
[14] A.A. Balandin, Thermal properties of graphene and nanostructured carbon materials, Nature Mater. 10 (2011) 569–581.
[15] R.K. Joshi, P. Carbone, F.C. Wang, V.G. Kravets, Y. Su, I.V. Grigorieva, H.A. Wu, A.K. Geim, R.R. Nair, Precise and ultrafast molecular sieving through graphene oxide membranes, Science 343 (2014) 752–754.
[16] J.N. Chen, M. Badioli, P. Alonso-Gonzalez, S. Thongrattanasiri, F. Huth, J. Osmond, M. Spasenovic, A. Centeno, A. Pesquera, P. Godignon, et al., Optical nano-imaging of gate-tunable graphene plasmons, Nature 487 (2012) 77–81.
[17] N.L. Yang, Y.Y. Liu, H. Wen, Z.Y. Tang, H.J. Zhao, Y.L. Li, D. Wang, Photocatalytic properties of graphdiyne and graphene modified TiO$_2$: from theory to experiment, ACS Nano 7 (2013) 1504–1512.
[18] H.J. Zhang, P.P. Xu, G.D. Du, Z.W. Chen, K. Oh, D.Y. Pan, Z. Jiao, A facile one-step synthesis of TiO$_2$/Graphene composites for photodegradation of methyl orange, Nano Res. 4 (2011) 274–283.
[19] E.P. Gao, W.Z. Wang, M. Shang, J.H. Xu, Synthesis and enhanced photocatalytic performance of graphene-Bi$_2$WO$_6$ composite, Phys. Chem. Chem. Phys. 13 (2011) 2887–2893.
[20] M. Nawaz, W. Miran, J. Jang, D.S. Lee, One-step hydrothermal synthesis of porous 3D reduced graphene oxide/TiO$_2$ aerogel for carbamazepine photodegradation in aqueous solution, Appl. Catal. B-Environ. 203 (2017) 85–95.
[21] M. Minella, F. Sordello, C. Minero, Photocatalytic process in TiO$_2$/graphene hybrid materials. Evidence of charge separation by electron transfer from reduced graphene oxide to TiO$_2$, Catal. Today 281 (2017) 29–37.
[22] W. Wang, X.G. Huang, M. Lai, C.H. Lu, RGO/TiO$_2$ nanosheets immobilized on magnetically actuated artificial cilia film: a new mode for efficient photocatalytic reaction, RSC Adv. 7 (2017) 10517–10523.
[23] Z.J. Li, Y. Qu, K. Hu, M. Humayun, S.Y. Chen, L.Q. Jing, Improved photoelectrocatalytic activities of BiOCl with high stability for water oxidation and MO degradation by coupling RGO and modifying phosphate groups to prolong carrier lifetime, Appl. Catal. B-Environ. 203 (2017) 355–362.
[24] X.J. Bai, C.P. Sun, D. Liu, X.H. Luo, D. Li, J. Wang, N.X. Wang, X.J. Chang, R.L. Zong, Y.F. Zhu, Photocatalytic degradation of deoxynivalenol using graphene/ZnO hybrids in aqueous suspension, Appl. Catal. B-Environ. 204 (2017) 11–20.
[25] R. Beura, P. Thangadurai, Structural, optical and photocatalytic properties of graphene-ZnO nanocomposites for varied compositions, J. Phys. Chem. Solids 102 (2017) 168–177.
[26] J.Q. Qin, X.Y. Zhang, C.W. Yang, M. Cao, M.Z. Ma, R.P. Liu, ZnO microspheres-reduced graphene oxide nanocomposite for photocatalytic degradation of methylene blue dye, Appl. Surf. Sci. 392 (2017) 196–203.
[27] H.R. Azimi, M. Ghoranneviss, S.M. Elahi, R. Yousefi, Photovoltaic and UV detector applications of ZnS/rGO nanocomposites synthesized by a green method, Ceram. Int. 42 (2016) 14094–14099.
[28] L. Kashinath, K. Namratha, K. Byrappa, Sol–gel assisted hydrothermal synthesis and characterization of hybrid ZnS-RGO nanocomposite for efficient photodegradation of dyes, J. Alloys Compd. 695 (2017) 799–809.
[29] Y. Feng, N.N. Feng, G.Y. Zhang, G.X. Du, One-pot hydrothermal synthesis of ZnS-reduced graphene oxide composites with enhanced photocatalytic properties, CrystEngComm 16 (2014) 214–222.
[30] M. Sookhakiana, Y.M. Amina, R. Zakaria, W.J. Basirun, M.R. Mahmoudian, B. Nasiri-Tabrizi, S. Baradaran, Majid Azarang, Significantly improved photocurrent response of ZnS-reduced graphene oxide composites, J. Alloys Compd. 632 (2015) 201–207.
[31] G. Sharma, S.W. Gosavi, Thermoluminescence properties of graphene-nano ZnS composite, J. Lumin. 145 (2014) 557–562.
[32] W. Qin, D.S. Li, X.J. Zhang, D. Yan, B.W. Hu, L.K. Pan, ZnS nanoparticles embedded in reduced graphene oxide as high performance anode material of sodium-ion batteries, Electrochim. Acta 191 (2016) 435–443.
[33] C. Xu, X. Wang, J.W. Zhu, Graphene-metal particle nanocomposites, J. Phys. Chem. C 112 (2008) 19841–19845.

[34] Y. Lei, F.F. Cheng, R. Li, J. Xu, A facile solvothermal method to produce graphene-ZnS composites for superior photoelectric applications, Appl. Surf. Sci. 308 (2014) 206–210.

[35] M. Sookhakiana, Y.M. Amina, W.J. Basirunb, Hierarchically ordered macro-mesoporous ZnS microsphere with reduced graphene oxide supporter for a highly efficient photodegradation of methylene blue, Appl. Surf. Sci. 283 (2013) 668–677.

[36] C. Nethravathi, T. Nisha, N. Ravishankar, C. Shivakumara, M. Rajamathi, Graphene-nanocrystalline metal sulphide composites produced by a one-pot reaction starting from graphite oxide, Carbon 47 (2009) 2054–2059.

[37] H.T. Hu, X.B. Wang, F.M. Liu, J.C. Wang, C.H. Xu, Rapid microwave-assisted synthesis of graphene nanosheets-zinc sulfide nanocomposites: optical and photocatalytic properties, Synth. Met. 161 (2011) 404–410.

[38] Y.J. Li, X.D. Li, J.W. Li, J. Yin, Photocatalytic degradation of methyl orange by TiO_2-Coated activated carbon and kinetic study, Water Res. 40 (2006) 1119–1126.

[39] X.Q. An, J.C. Yu, Graphene-based photocatalytic composites, RSC Adv. 1 (2011) 1426–1434.

[40] H. Zhang, X.J. Lv, Y.M. Li, P25-graphene composite as a high performance photocatalyst, ACS Nano 4 (2010) 380–386.

[41] J.S. Lee, K.H. You, C.B. Pack, Highly photoactive, low bandgap TiO_2 nanoparticles wrapped by graphene, Adv. Mater. 24 (2012) 1084–1088.

[42] Y.H. Zhang, N. Zhang, Z.R. Tang, Y.J. Xu, Graphene transforms wide band gap ZnS to a visible light photocatalyst. The new role of graphene as a macromolecular photosensitizer, ACS Nano 6 (2012) 9777–9789.